Published in final edited form as:
Hum Mol Genet. 2008 March 1; 17(5): 631–641. doi:10.1093/hmg/ddm188.

Disruption of the *Flnb* gene in mice phenocopies the human disease spondylocarpotarsal synostosis syndrome

Claire Farrington-Rock[1], **Veneta Kirilova**[1], **Lisa Dillard-Telm**[2], **Alexander D. Borowsky**[2,3], **Sara Chalk**[2], **Matthew J. Rock**[1], **Daniel H. Cohn**[1,4,5], and **Deborah Krakow**[1,4,6,*]

1 *Medical Genetics Institute, Cedars-Sinai Medical Center, 8700 Beverly Boulevard, SSB-371, Los Angeles, CA 90048, USA*

2 *Center for Comparative Medicine and Mouse Biology Program, UC Davis School of Medicine, Davis, CA 95616, USA*

3 *Department of Pathology and Laboratory Medicine, UC Davis School of Medicine, Davis, CA 95616, USA*

4 *Department of Human Genetics, David Geffen School of Medicine at UCLA, Los Angeles, CA 90095, USA*

5 *Department of Pediatrics, David Geffen School of Medicine at UCLA, Los Angeles, CA 90095, USA*

6 *Department of Obstetrics and Gynecology, David Geffen School of Medicine at UCLA, Los Angeles, CA 90095, USA*

Abstract

Spondylocarpotarsal synostosis syndrome (SCT) is an autosomal recessive disease that is characterized by short stature, and fusions of the vertebrae and carpal and tarsal bones. SCT results from homozygosity or compound heterozygosity for nonsense mutations in *FLNB. FLNB* encodes filamin B, a multifunctional cytoplasmic protein that plays a critical role in skeletal development. Protein extracts derived from cells of SCT patients with nonsense mutations in *FLNB* did not contain filamin B, demonstrating that SCT results from absence of filamin B. To understand the role of filamin B in skeletal development, an $Flnb^{-/-}$ mouse model was generated. The $Flnb^{-/-}$ mice were phenotypically similar to individuals with SCT as they exhibited short stature and similar skeletal abnormalities. Newborn $Flnb^{-/-}$ mice had fusions between the neural arches of the vertebrae in the cervical and thoracic spine. At postnatal day 60, the vertebral fusions were more widespread and involved the vertebral bodies as well as the neural arches. In addition, fusions were seen in sternum and carpal bones. Analysis of the $Flnb^{-/-}$ mice phenotype showed that an absence of filamin B causes progressive vertebral fusions, which is contrary to the previous hypothesis that SCT results from failure of normal spinal segmentation. These findings suggest that spinal segmentation can occur normally in the absence of filamin B, but the protein is required for maintenance of intervertebral, carpal and sternal joints, and the joint fusion process commences antenatally.

INTRODUCTION

Spondylocarpotarsal synostosis syndrome (SCT) (OMIM: 272460) is an autosomal recessive disease that is characterized by fusions of the vertebrae and carpal and tarsal bones. Affected individuals have short stature with a disproportionately short trunk, lordosis and/or scoliosis, delayed bone age, occasional cleft palate, sensorineural or mixed hearing loss and enamel hypoplasia (1–3). Different types of vertebral fusions have been described: those involving the

*To whom correspondence should be addressed. Tel: +1 3104236460; Fax: +1 3104230620; Email: E-mail: deborah.krakow@cshs.org.

Conflict of Interest statement. The authors declare that they have no conflicting interests.

posterior elements (spinal processes) only and those with unilateral and bilateral fusions of entire vertebrae. The vertebral fusions seen in the SCT patients have been hypothesized to result from failure of normal spinal segmentation or somitogenesis (1–4).

SCT results from homozygosity or compound heterozygosity for nonsense mutations in *FLNB* (OMIM: 603381) that predict a loss of functional protein (4). Heterozygosity for structural mutations in *FLNB* are also known to cause a spectrum of autosomal dominant skeletal disorders, including Larsen syndrome (OMIM: 150250), atelosteogenesis type I (OMIM: 108720), atelosteogenesis type III (OMIM: 108721) and Boomerang dysplasia (OMIM: 112310) (4–7). While there are some phenotypic similarities between autosomal recessive SCT and the aforementioned autosomal dominant disorders, the mode of inheritance and predicted effects on the protein distinguish these disorders.

FLNB encodes filamin B, a 280 kDa multifunctional cytoplasmic protein (8). Filamin B is a member of a family of proteins that also includes filamins A and C. The three filamins are very similar to each other and share the same modular structure (Fig. 1A); two calponin homology domains (CHD), also known as actin-binding domains (ABD), followed by 24 filamin repeat domains which are interrupted by two small hinge regions (9–11). Dimerization of filamin monomers at their carboxyl-terminal ends produces the functional protein (12). These paralogous proteins participate in cross-linking the actin cytoskeleton into gel networks or parallel bundles, link membrane proteins to the cytoskeleton and provide a scaffold for signaling molecules and small solutes. Though a ubiquitously expressed intracellular protein, the finding that a spectrum of mutations in *FLNB* produced a series of distinct skeletal dysplasias uncovered a critical role for filamin B in skeletal development.

To begin to understand the role of filamin B in skeletogenesis, an $Flnb^{-/-}$ mouse was generated using gene trap technology. $Flnb^{-/-}$ mice, similar to individuals with SCT, do not express full-length filamin B and their skeletal abnormalities recapitulate the human disease. The mice exhibit short stature, show progressive vertebral fusions and scoliosis, and have carpal fusions. Since this $Flnb^{-/-}$ mouse model phenocopies the human disorder, it provides insight into the underlying mechanism of disease in SCT and begins to dissect out the fundamental role filamin B has in skeletal development.

RESULTS

Identification of mutations in spondylocarpotarsal synostosis syndrome patients

SCT is a recessively inherited disease that can result from homozygosity or compound heterozygosity for nonsense mutations in *FLNB* [Table 1, Fig. 1; (4)]. To further define the molecular basis of SCT, three additional families were analyzed. In the first family, the parents were consanguineous and had three offsprings of which one was affected. The affected individual was found to be homozygous for the mutation c.5548G > T, predicted to create a translational termination codon (p.Gly1850X; Table 1, Patient 5) while both parents demonstrated heterozygosity for the mutation. The second family was not consanguineous and had a single affected child who was compound heterozygous for the mutations c.1945C > T and c.4671G > A (Table 1, Patient 6). The first of these changes predicted a premature translational termination codon (p.Arg649X) and was shown to be transmitted from the mother. The second mutation was in the last nucleotide of exon 27 and was found to be transmitted from the father. The nucleotide substitution G > A altered the exon 27 splice donor site. Analysis of the filamin B transcript amplified from the father and the affected offspring showed that the mutation resulted in abnormal splicing of exon 27 (Fig. 1B and C) which produced a frame-shift and predicted a premature translational termination codon (p.Ser1505-ArgfsX33). The third family was consanguineous and the affected child was found to be homozygous for

the mutation c.6010C > T, predicted to create a translational termination codon (p.Arg2004X; Table 1, Patient 7).

Filamin protein expression in spondylocarpotarsal synostosis syndrome families

The premature translational termination codons predicted in the SCT patients could lead to either expression of a truncated form of the filamin B protein or to transcripts subjected to nonsense-medicated decay and consequent absence of filamin B protein. To distinguish between these two possibilities, protein was isolated from lymphoblastoid cell lines available from three genetically independent SCT patients (Table 1) and filamin B expression levels were determined by western blotting. No full-length or truncated forms of filamin B were seen in the cell lines derived from patients with SCT (Fig. 2A). To test whether absence of filamin B had an effect on the paralogous filamin A levels, filamin A expression was also analyzed (Fig. 2B). Affected individuals expressed filamin A at similar levels as control individuals.

Generation of filamin B-deficient mice

Chimeric mice were generated from ES cell line RRF239 containing the insertional mutation of the gene-trap vector. 5′ RACE products from mRNA of RRF239 revealed that the gene-trap had inserted into intron 3 of *Flnb*. The insertion of the vector into intron 3 was predicted to produce a fusion transcript of exons 1–3 followed by the reporter *β-geo*, a fusion of the β-galactosidase and neomycin-resistance genes. Chimeric males were mated with female C57BL/6 mice to generate mice heterozygous for the gene-trap ($Flnb^{+/-}$). $Flnb^{+/-}$ mice were mated to generate mice homozygous for the gene-trap ($Flnb^{-/-}$).

The genotypes of the mice were determined by PCR reactions using genomic DNA and three different primer pairs (Fig. 3A and B). The first primer pair amplified a region within the β-galactosidase gene (Fig. 3A, 1F and 1R) allowing differentiation of wild-type mice ($Flnb^{+/+}$) (Fig. 3B, mouse 1) from the gene-trap mice. The other primers amplified sequences within intron 3 of *Flnb*, 5′ and 3′ to the gene-trap vector insertion site (Fig. 3A, 2F and 2R, 3F and 3R). These primers amplified a product if the gene-trap was absent and therefore $Flnb^{+/-}$ mice (Fig. 3B, mouse 2 and 3) and $Flnb^{-/-}$ mice (Fig. 2B, mouse 4) were differentiated. Analysis of ribcage protein extracts from newborn mice by western blot analysis revealed that $Flnb^{-/-}$ mice did not express full-length filamin B protein and the $Flnb^{+/-}$ mice expressed less than the $Flnb^{+/+}$ mice (Fig. 3C). In addition, the $Flnb^{-/-}$ mice expressed filamin A protein at similar levels as the $Flnb^{+/+}$ and $Flnb^{+/-}$ mice (Fig. 3C).

Expression of filamin B in developing embryos

The presence of the β-galactosidase gene in the gene-trap vector was utilized to determine the expression profile of filamin B protein during development. $Flnb^{+/-}$ embryos at different gestational ages were stained for β-galactosidase enzyme activity in either the intact embryos (Fig. 4A and B) or in tissue sections (Fig. 4C and D). No expression was seen in the control $Flnb^{+/+}$ mice (Fig. 4B) showing that activity was only present with the gene-trap vector. In $Flnb^{+/-}$ embryos at E10.5, β-galactosidase activity was detected in the forelimb bud, in the frontal and hind regions of the developing calvarium and also in the developing heart (not shown). At E12.5 expression was localized to the developing skeletal elements of the $Flnb^{+/-}$ mice (Fig. 4A). Analysis of tissue sections showed expression of filamin B in the precartilage primordia of the developing limbs (Fig. 4C), neural arches of the vertebrae and ribs (Fig. 4D) and the skull bones (not shown). By E14.5, expression remained localized to the skeletal elements, but diminished expression was seen in the scapula, humeri and ribs, and frontal calvarium expression was now absent (not shown).

Phenotype of *Flnb*$^{-/-}$ mice

Mice were generated by *Flnb*$^{+/-}$ intercrosses; so phenotypic comparisons could be made between different genotypes at two main time points—birth and postnatal day 60. The pups studied at birth were taken from eight independent litters and were collected as close to delivery as possible. Some of the pups were dead when the litters were collected, however milk was observed in their stomachs suggesting they were live born and initially able to feed. The newborn litters had an equal number of male and female mice and genotypes were close to the expected Mendelian ratios (*Flnb*$^{+/+}$ 17%:*Flnb*$^{+/-}$ 57%:*Flnb*$^{-/-}$ 26%; $n = 47$), however, nearly 50% of the *Flnb*$^{-/-}$ pups were dead at collection. At postnatal day 60, mice were taken from 20 independent litters. These mice were genotyped at postnatal day 21 (i.e. at weaning), and the genotyping results revealed a greater loss of *Flnb*$^{-/-}$ mice (*Flnb*$^{+/+}$ 31%:*Flnb*$^{+/-}$ 64%:*Flnb*$^{-/-}$ 5%; $n = 102$), indicating that a majority of the *Flnb*$^{-/-}$ mice died within the first few days of life. Weights of newborn pups revealed that *Flnb*$^{-/-}$ mice were significantly smaller than their littermates (Fig. 5A), but there were no other gross observable differences between the *Flnb*$^{-/-}$ *mice and either the Flnb*$^{+/+}$ or *Flnb*$^{+/-}$ mice. The differences in weight corresponded to an overall difference in size, which could be seen by skeletal preparation at the newborn period (Fig. 5B) and in adulthood. Weights were recorded over a 3-week post-weaning period and showed that *Flnb*$^{-/-}$ mice were consistently smaller than their littermates (Fig. 5C). The *Flnb*$^{-/-}$ mice were also distinguishable from their littermates as they developed an ‘hourglass’ body shape and had restricted upper body movement that caused them to walk with what could be described as a ‘swagger’ or ‘waddle’.

Analysis of the newborn *Flnb*$^{-/-}$ skeletal preparations revealed aberrant mineralization in the neural arches leading to fusions between individual vertebrae (Fig. 6A and C). Fusions were seen in the neural arches unilaterally and bilaterally, and were observed in the vertebrae of the cervical and thoracic regions (Fig. 6C and D). In the neural arches of thoracic vertebrae that had not undergone mineralization, the cartilaginous tissue of the superior and inferior articular processes were fused together (Fig. 6B). No changes in mineralization were seen in the centra of the vertebrae (Fig. 6A and C) or in any other areas of the skeleton at this time point. Histological analysis revealed no gross disruption in the organization of long bone growth plate cartilage or in the lengths of the hypertrophic, proliferative or resting or reserve zones of the growth plate (Fig. 6E).

Analysis of the postnatal day 60 skeletal preparations revealed vertebral fusions in the *Flnb*$^{-/-}$ mice throughout the cervical, thoracic and lumbar regions of the spine (Fig. 7A–C); however, the sacral vertebrae were fused normally (Fig. 7B) and no fusions were seen in the caudal region. Fusions were seen along the dorsal and ventral sides of the spine (Fig. 7B and C), including the centra. In some regions individual vertebrae could not be distinguished as they appeared as one unified block, however, in most of the vertebrae individual neural and transverse process could be distinguished even when the neural arches had fused. The vertebral fusions produced scoliosis and a generalized flattening of the spine and contributed significantly to the short stature of the *Flnb*$^{-/-}$ mice. Fusions were also identified in the sternum of the *Flnb*$^{-/-}$ mice between all sternebrae and the manubrium (Fig. 7D). Micro-CT analysis of the *Flnb*$^{-/-}$ mice demonstrated carpal fusions (Fig. 7E). In all *Flnb*$^{-/-}$ mice analyzed, fusions were between the second distal carpal, centrale and the third distal carpal. In some *Flnb*$^{-/-}$ mice, fusion was also observed between the fused radiale and intermedium and the ulnare (Fig. 7E).

DISCUSSION

SCT is an autosomal recessive skeletal dysplasia characterized by fusions of the vertebrae and carpal and tarsal bones (1–3). The genetic basis of SCT has been demonstrated to result from nonsense mutations in *FLNB* (4). To corroborate these findings, three new cases of SCT were

analyzed for *FLNB* mutations. In concordance with previous data, affected individuals were either homozygous or compound heterozygous for *FLNB* nonsense mutations (Table 1). All of the mutations were novel except for the heterozygous change c.1945C > T in Patient 6 which was found as a homozygous change in Patient 1. The ethnic backgrounds (Patient 1 Hispanic, Patient 6 Caucasian) indicated they are unrelated and that the recurrence of this mutation is probably not due to a founder effect in a particular population. The nonsense mutations found in *FLNB* predict the introduction of premature translational termination codons which could either lead to the expression of a truncated form of filamin B or to transcripts subjected to nonsense-mediated decay and consequent absence of filamin B protein. Protein extracts taken from SCT patient cell lines did not express full length or truncated filamin B protein (Fig. 2A), thereby demonstrating that SCT results from absence of filamin B. As the filamins comprise a homologous family of proteins the hypothesis that absence of filamin B may affect the expression of filamin A, which is also ubiquitously expressed, was tested. No significant effect on filamin A expression was detected in SCT patients (Fig. 2B) suggesting no compensatory role for filamin A.

To understand the disease mechanism of SCT and the role of filamin B in skeletogenesis, an *Flnb*$^{-/-}$ mouse was generated using gene-trap technology. Because of the presence of *β-geo* in the gene-trap vector, the expression pattern of filamin B could be studied during development. Filamin B expression was detected at all time points analyzed and was predominantly expressed with the developing bones (Fig. 4), confirming an important role for filamin B in skeletogenesis. At E12.5, the developing mouse skeleton consisted of precartilaginous condensations, and filamin B expression was predominantly localized to these regions. By E14.5, the precartilaginous tissue had differentiated into cartilage and there were multiple centers of ossification. At this stage, filamin B expression was present in the cartilage, but not in areas of mineralized bone, such as the scapula, humeri, ribs and frontal calvarium. The expression pattern described indicates an important function for filamin B throughout chondrogenesis, but not in mature bone. These findings confirm previous data that localized filamin B to the condensing chondrocytes of embryonic mouse vertebrae and also within the epiphyseal growth plate cartilage of human fetal femurs (4).

The *Flnb*$^{-/-}$ mice were phenotypically similar to individuals with SCT as they exhibited skeletal abnormalities seen in the human disease (Fig. 7). Newborn *Flnb*$^{-/-}$ mice had unilateral and bilateral fusions between the neural arches of the vertebrae in the cervical and thoracic spine (Fig. 6). These fusions were present as mineralized tissue between adjacent neural arches and as fused cartilage between the superior and inferior articular processes. It is unclear whether these findings reflect an over production of cartilaginous tissue which can differentiate into mineralized tissue or whether the cartilaginous tissue is unable to undergo apoptosis and proper joint formation. At postnatal day 60, vertebral fusions were more widespread and involved cervical, thoracic and lumbar vertebrae (Fig. 7). The vertebral fusions in SCT patients are also present in the cervical, thoracic and lumbar regions of the spine. Different types of fusions were observed in the *Flnb*$^{-/-}$ mice including those between the neural arches only and those involving the entire vertebrae, both bilaterally and unilaterally, the latter resulting in wedged vertebrae and causing scoliosis (Fig. 7). Similarly, all of these different types of fusions have been described in SCT patients (2). In addition to the vertebral fusions, fusions were also seen in the sternum and carpal bones of *Flnb*$^{-/-}$ mice. Carpal fusions are always present in SCT patients, and the fusions can occur between different carpal bones (the hamate and capitate or the lunate and triquetrum), and are seen unilaterally or bilaterally (1–3). The presence of sternal fusions has never been reported in SCT patients. However, it is possible that SCT patients have fused sternums and the use of current CT for clinical spinal assessment could be used to determine this.

The *Flnb*$^{-/-}$ mice were also similar to humans with SCT in that they were smaller than their littermates at birth and remained smaller throughout life (Fig. 5). At birth, SCT patients are usually between the 10th and 50th centile for length, below average but still considered to be within the normal range. However, in childhood and adulthood, all SCT patients are reported to be below the third centile for height (1,3,13,14), demonstrating that most of the decreased growth is postnatal. The reduced height of SCT patients probably results from progressive vertebral fusions as they have a characteristic disproportionately short trunk. Similarly, in the *Flnb*$^{-/-}$ mice, it appeared that vertebral fusions were the main contributor to their short stature. Whether abnormalities in the appendicular skeleton contributed to the short stature could not be definitively determined by measuring the long bones of newborn mice. Similarly, the growth plates of the P1 mice did not show any gross abnormalities. At postnatal day 60, there was no difference in femur length of *Flnb*$^{-/-}$ mice when compared with their normal littermates.

In accord with Mendelian ratios, *Flnb*$^{+/-}$ intercrosses generated the expected number of *Flnb*$^{-/-}$ mice, however a majority of them died in the first few days of life. The reason for the postnatal loss is unknown. It is possible that the mothers rejected the *Flnb*$^{-/-}$ mice because they were smaller than the rest of the litter and therefore suspected to be unhealthy. Alternatively, the loss of *Flnb*$^{-/-}$ mice may result from the vertebral fusions restricting normal growth of the spine, leading to spinal cord compression and/or respiratory insufficiency.

A different *Flnb*-deficient mouse model has been reported and was generated using a gene-trap vector that was inserted into intron 20 of *Flnb* (15). In this model, a majority of the *Flnb*$^{-/-}$ mice died after E11.5 due to impaired development of the microvasculature as well as alterations in skeletal system. The mice were kyphotic and had reduction of hyaline cartilage in the ribs, metacarpals, phalanges and tarsals, but no fusions were reported in the carpals or tarsals. Vertebral fusions were present, but were thought to occur due to the absence of intervertebral discs. The long bones were shorter, had reduced bone mineral density and reduced cortical thickness. The phenotypic differences between the mouse model described here and the one described by Zhou *et al*. may be due to the different fusion proteins generated by the position of the gene-trap vector. In the intron 3 gene-trap model, the *Flnb*$^{-/-}$ mice would be expected to express a protein containing most of the ABD fused to β-geo, likely a non-functional protein. The intron 20 gene-trap could express all of the ABD and the first eight filamin repeat domains fused to β-geo. Although the carboxyl-terminal dimerization domain is not predicted to be expressed in either model, perhaps the longer fusion product of the intron 20 gene-trap retains some activity. On phenotypic grounds, it appears that the intron 3 gene-trap model more closely resembles human SCT.

The vertebral fusions observed in SCT patients have been hypothesized to result from either failure of normal somitogenesis or defective spinal segmentation during development (1–4). Despite the neural arch fusions in the newborn *Flnb*$^{-/-}$ mice, no fusions were observed between the centra and segmentation of the vertebrae appeared normal (Fig. 5). Comparisons between the newborn and postnatal day 60 mice indicate that the fusions are a progressive process. These findings suggest that spinal segmentation occurs normally in the absence of filamin B, but the protein is required for maintenance of intervertebral, carpel and sternal joints and the joint fusion process commences antenatally.

MATERIALS AND METHODS

Mutation detection in FLNB

Under an approved IRB protocol DNA samples were collected from patients with SCT referred through the International Skeletal Dysplasia Registry (ISDR). Each diagnosis was confirmed by clinical and radiographic criteria. Genomic DNA was used to amplify PCR fragments covering the entire coding sequence of *FLNB* using a Gene Amp® PCR System 9700 (Applied

Biosystems, Foster City, CA, USA). PCR products were sequenced using the ABI Prism Big-Dye® Terminator Cycle Sequencing Kit, version 3.1 (Applied Biosystems) and analyzed on an ABI Prism™ 377 DNA Sequencer (Applied Biosystems). Sequence data were processed using ABI software and analyzed using Sequencher (Gene Codes, www.genecodes.com). DNA sequences were compared with the *FLNB* cDNA (GenBank accession code NM_001457) and nucleotide numbering started at translation initiation (corresponding to the A of the ATG translation initiation codon in the reference sequence). Mutations were confirmed from two separate PCR products and bi-directional sequencing.

Immunoblotting

For filamin A and B expression studies in SCT patients, protein was extracted from lymphoblastoid cell lines into RIPA buffer and resolved under reduced conditions on a 6% SDS–PAGE gel. Proteins were transferred onto a nitrocellulose membrane and blocked overnight in 5% (w/v) powdered milk in PBS containing 0.1% (v/v) Tween-20 (PBS-T). Membranes were incubated with either anti-human filamin B rabbit polyclonal antibody raised against H1 (kind gift from Dr Shapiro, Thomas Jefferson University) or the H2 (Chemicon), or the anti-filamin A monoclonal antibody (Lab Vision Corporation) for 1 h at room temperature. The membranes were washed and incubated with an HRP-conjugated antibody (Cell Signaling Technology, Inc.) in 5% milk in PBS-T. The membranes were washed again and immunoreactivity was detected using enhanced chemiluminescence (Amersham BioSciences). For expression studies of filamin B in mice, protein was isolated from newborn sternum including adjacent non-mineralized rib tissue. Tissue was snap-frozen, ground in a mortar and pestle and the tissue mixed end-over-end with RIPA buffer for 24 h at 4°C. Extracted proteins were analyzed as detailed above.

Generation of mice

An ES cell line from the BayGenomics database (http://baygenomics.ucsf.edu) was identified containing a gene-trap in *Flnb*. ES cell line RRF239 (strain 129P2) contained the gene-trap vector pGT0Lxf inserted into intron 3 of *Flnb*. RRF239 cells were microinjected into C57BL/6 (The Jackson Laboratory) blastocysts to generate chimeras. Male chimeras were mated with female C57BL/6 mice to generate $Flnb^{+/-}$ mice. The mice used in the study were maintained on a mixed background.

Genotyping of $Flnb^{-/-}$ mice

Genotyping of mice was determined by three parallel PCR reactions. Gene-trap mice were distinguished from wild-type mice using β-galactosidase-specific oligonucleotides: 1F (5′-TTATCGATGAGCGTGGTGGTTATGC-3′) and 1R (5′-GCGCGTACATCGGGCAAATAATATC-3′). $Flnb^{+/-}$ mice were distinguished from $Flnb^{-/-}$ mice using two oligonucleotide pairs specific to sequences within intron 3 of *Flnb*: 2F (5′-TGCTCCATGACCATTCTCAG-3′) and 2R (5′-AGTGAGGTCCTGGCTCAAAA-3′); 3F (5′-ACCAGTCCCATGGATCAGAG-3′) and 3R (5′-CACTCCCCTGGT CACGTATT-3′). PCR was carried out using standard techniques and conditions were 35 cycles at 96°C for 10 s, 55°C for 20 s and 72°C for 2 min. Genomic DNA was isolated from kidney of newborn mice or from the tail tips of 21-day-old mice using DNeasy Tissue Kit (Qiagen).

β-Galactosidase staining of embryos

β-Galactosidase staining of the *β-geo* reporter was performed by whole embryo fixation in neutral-buffered formalin pH 7.0 for 1 h at 4°C. Embryos were rinsed in 100 mM $NaPO_4$ pH 7.3 containing 2 mM $MgCl_2$, 0.01% SDS and 0.02% NP-40 for 30 min three times. The embryos were then stained overnight in 100 mM $NaPO_4$ pH 7.3 containing 2 mM $MgCl_2$, 0.01% SDS, 0.02% NP-40, 5 mM $K_3[Fe(CN)_6]$, 5 mM $K_4[Fe(CN)_6] \cdot 3H_2O$ and 1 mg/ml X-

gal. Embryos were cleared in formalin overnight at 4°C, washed twice in distilled H_2O for 30 min each, dehydrated in graded ethanol (70% for 30 min, 95% for 30 min and twice in 100% for 30 min each) and transferred to methyl salicylate for photography and storage.

Skeletal preparations of newborn and adult mice

Euthanized newborn mice were eviscerated, all organs were removed from the body cavity and the remaining tissue was fixed in 95% ethanol for 3 days. The fixed mice were stained with 0.015% alcian blue 8GX (Sigma–Aldrich, St Louis, MO, USA) in 75% ethanol and 20% glacial acetic acid for 3 days and then destained for at least 6 h in 95% ethanol. The remaining soft tissue was digested by incubating with 2% KOH for 24 h. The skeleton was stained with 0.005% alizarin red S (Sigma–Aldrich) in 1% KOH for 24 h and then destained, first with 2% KOH for 24 h and then with 1% KOH in 20% glycerol until all of the residual stain was removed. The final skeletal preparations were stored in a 1:1 solution of glyerol:ethanol. For mice sacrificed at postnatal day 60, a similar protocol was used with the following modifications. During the initial dissection, as much muscle as possible was dissected from the skeleton. The remaining tissue was fixed for 1 week before staining with alcian blue for 5 days. The soft tissue was digested in 2% KOH for 3 days before staining with alizarin red S.

Micro-CT analysis of mice

Analysis was performed on newborn and postnatal day 60 skeletal preparations using a micro-CT scanner (micro CT-40, Scanco, Switzerland). Samples were placed into the holder in 1% KOH containing 20% glycerol along with gauze to hold them in place. Scanning data were collected in 20 μm sections and an optimum threshold was calculated using the two-dimensional images which was applied to comparative samples. These data were used to carry out three-dimensional reconstructions of the skeletal preparations.

Acknowledgements

The authors wish to thank the families and their physicians for participating in the studies described here and Robert J. Munn for help with photography. The work was supported in part by grants from the NIH (HD22657 and RR00425 to D.H.C. and D.K.), NCRR/NIH (U42 RR14905 for A.D.B.) and the Joseph Drown Foundation (to D.K.). D.H.C. and D.K. are recipients of Winnick Family Clinical Scholar Awards.

References

1. Wiles CR, Taylor TFK, Sillence DO. Congenital synspondylism. Am J Med Genet 1992;42:288–295. [PubMed: 1536163]
2. Langer LO Jr, Gorlin RJ, Donnai D, Hamel BC, Clericuzio C. Spondylocarpotarsal synostosis syndrome (with or without unilateral unsegmented bar). Am J Med Genet 1994;51:1–8. [PubMed: 8030662]
3. Coêlho KEFA, Ramos ES, Felix TM, Martelli L, de Pina-Neto JM, Niikawa N. Three new cases of spondylocarpotarsal synostosis syndrome: clinical and radiographic studies. Am J Med Genet 1998;77:12–15. [PubMed: 9557886]
4. Krakow D, Robertson SP, King LM, Morgan T, Sebald ET, Bertolotto C, Wachsmann-Hogiu S, Acuna D, Shapiro SS. Mutations in the gene encoding filamin B disrupt vertebral segmentation, joint formation and skeletogenesis. Nat Genet 2004;36:405–410. [PubMed: 14991055]
5. Bicknell LS, Morgan T, Bonafé L, Wessels MW, Bialer MG, Willems PJ, Cohn DH, Krakow D, Robertson SP. Mutations in *FLNB* cause boomerang dysplasia. J Med Genet 2005;42:e43. [PubMed: 15994868]
6. Farrington-Rock C, Firestein MH, Bicknell LS, Superti-Furga A, Bacino CA, Cormier-Daire V, Le Merrer M, Baumann C, Roume J, Rump P, et al. Mutations in two regions of *FLNB* result in atelosteogenesis I and III. Hum Mutat 2006;27:705–710. [PubMed: 16752402]

7. Bicknell LS, Farrington-Rock C, Shafeghati Y, Rump P, Alanay Y, Alembik Y, Al-Madani N, Firth H, Karimi-Nejad MH, Kim CA, et al. A molecular and clinical study of Larsen syndrome caused by mutations in *FLNB*. J Med Genet 2007;44:89–98. [PubMed: 16801345]
8. Takafuta T, Wu G, Murphy GF, Shapiro SS. Human beta-filamin is a new protein that interacts with the cytoplasmic tail of glycoprotein Ibalpha. J Biol Chem 1998;273:17531–17538. [PubMed: 9651345]
9. van der Flier A, Sonnenberg A. Structural and functional aspects of filamins. Biochem Biophys Acta 2001;1538:99–117. [PubMed: 11336782]
10. Stossel TP, Condeelis J, Cooley L, Hartwig JH, Noegel A, Schleicher M, Shapiro SS. Filamins as integrators of cell mechanics and signalling. Nat Rev Mol Cell Biol 2001;2:138–145. [PubMed: 11252955]
11. Popowicz GM, Schleicher M, Noegel AA, Holak TA. Filamins: promiscuous organizers of the cytoskeleton. TIBS 2006;31:411–419. [PubMed: 16781869]
12. Pudas R, Kiema TR, Butler PJG, Stewart M, Ylänne J. Structural basis for vertebrate filamin dimerization. Structure 2005;13:111–119. [PubMed: 15642266]
13. Steiner CE, Torriani M, Norato DYJ, Marques-de-Faria AP. Spondylocaroptarsal synostosis with ocular findings. Am J Med Genet 2000;91:131–134. [PubMed: 10748412]
14. Honeywell C, Langer L, Allanson J. Spondylocaroptarsal synostosis with epiphyseal dysplasia. Am J Med Genet 2002;109:318–322. [PubMed: 11992487]
15. Zhou X, Tian F, Sandzen J, Cao R, Flaberg E, Szekely L, Cao Y, Ohlsson C, Bergo MO, Boren J, Akyurek LM. Filamin B deficiency in mice results in skeletal malformations and impaired microvascular development. Proc Natl Acad Sci 2007;104:3919–3924. [PubMed: 17360453]

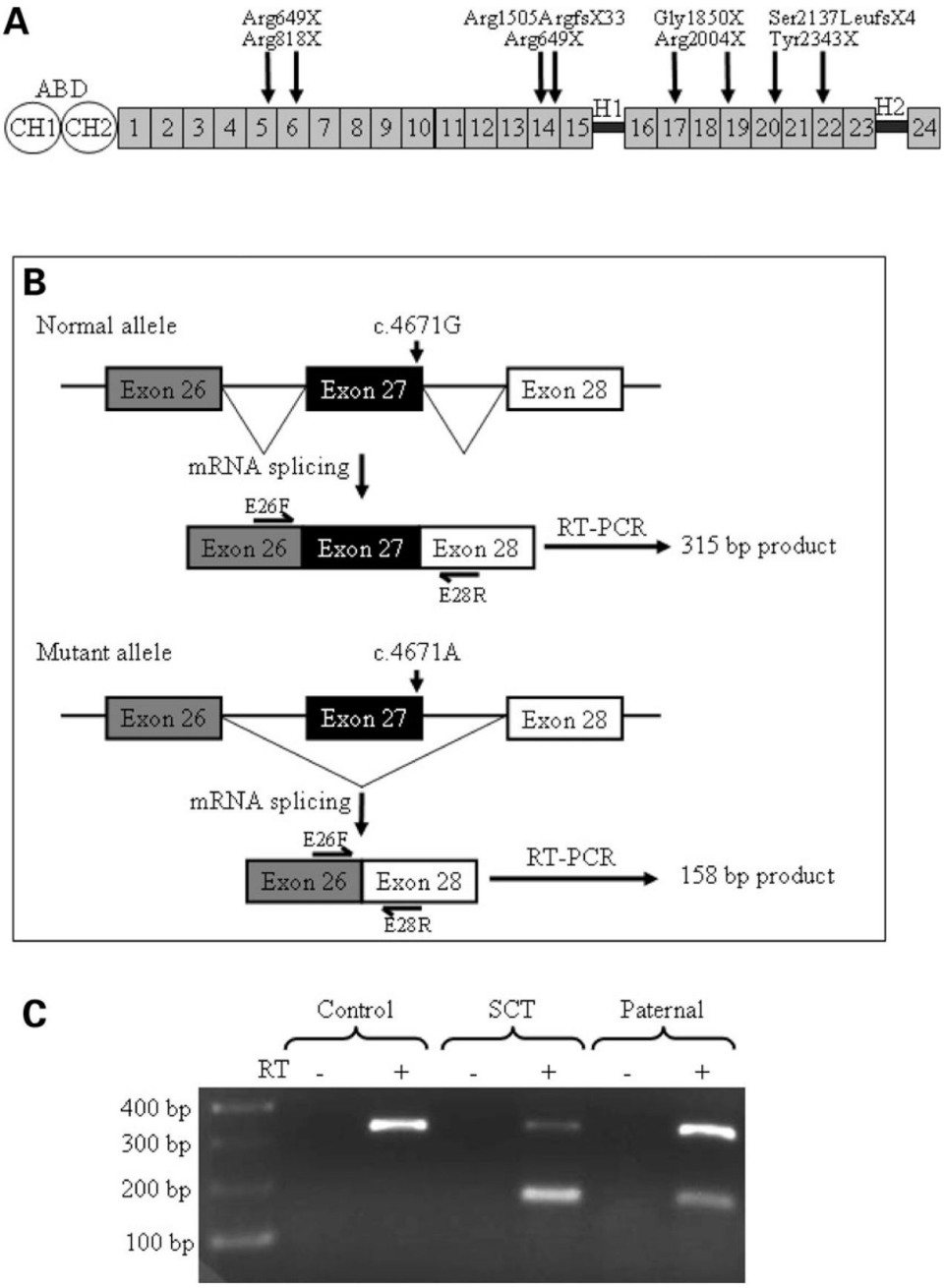

Figure 1.

(**A**) Diagrammatic representation of the filamin B protein. The arrows indicate the location of the mutations predicted to produce SCT. At the amino-terminal end is the actin-binding domain (ABD) comprised of two calponin-homology regions, CH1 and CH2. The remaining portion of the molecule is composed of 24 repeat structures, interrupted by two small hinge regions, H1 and H2. (**B**) Diagrammatic representation demonstrating that the mutation c.4671G > A in exon 27 of Patient 6 altered the exon 27 splice donor site and led to altered splicing of exon 27 from the filamin B transcript. RT–PCR products were generated using primers designed to sequences in exon 26 (E26F) and exon 28 (E28R) and predicted a 315 bp product if the transcript contained exon 27 or 158 bp product if exon 27 was spliced from the transcript.

(**C**) RT–PCR analysis of the filamin B transcript amplified from control, Patient 6 and the father of Patient 6 and using the amplification scheme described in (B). The control had the 315 bp product showing the presence of exon 27 in the transcript. Patient 6 and the father of Patient 6 (paternal) amplified a product of 315 and 158 bp showing that exon 27 was spliced from some of the filamin B transcript.

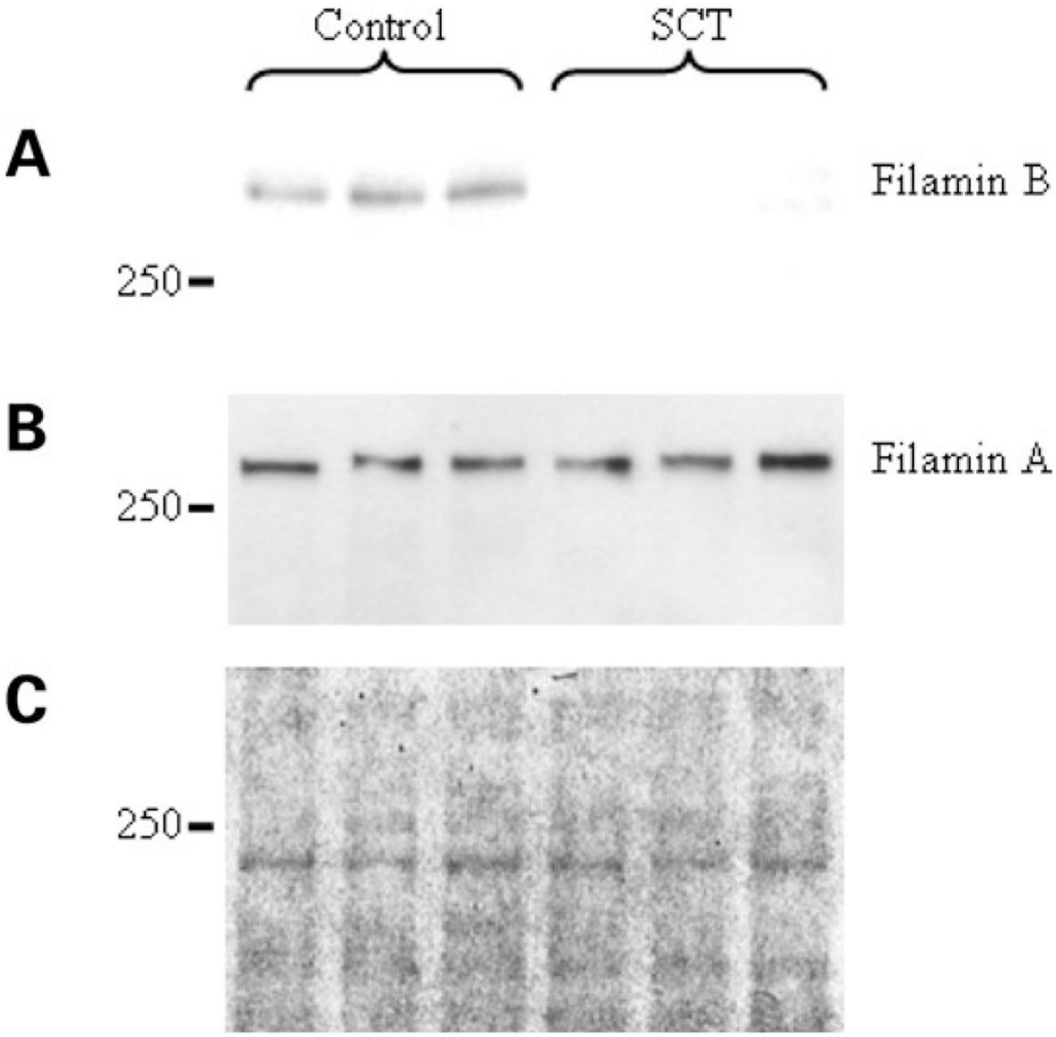

Figure 2.
Western blot analysis of filamin B (**A**) and filamin A (**B**) expression from lymphoblastoid cell line extracts from normal controls (lanes 1–3) and SCT patients (lanes 4–6). A coomassie blue-stained SDS–PAGE gel of the extracts used in the western blot to demonstrate the total protein loaded onto the gel (**C**).

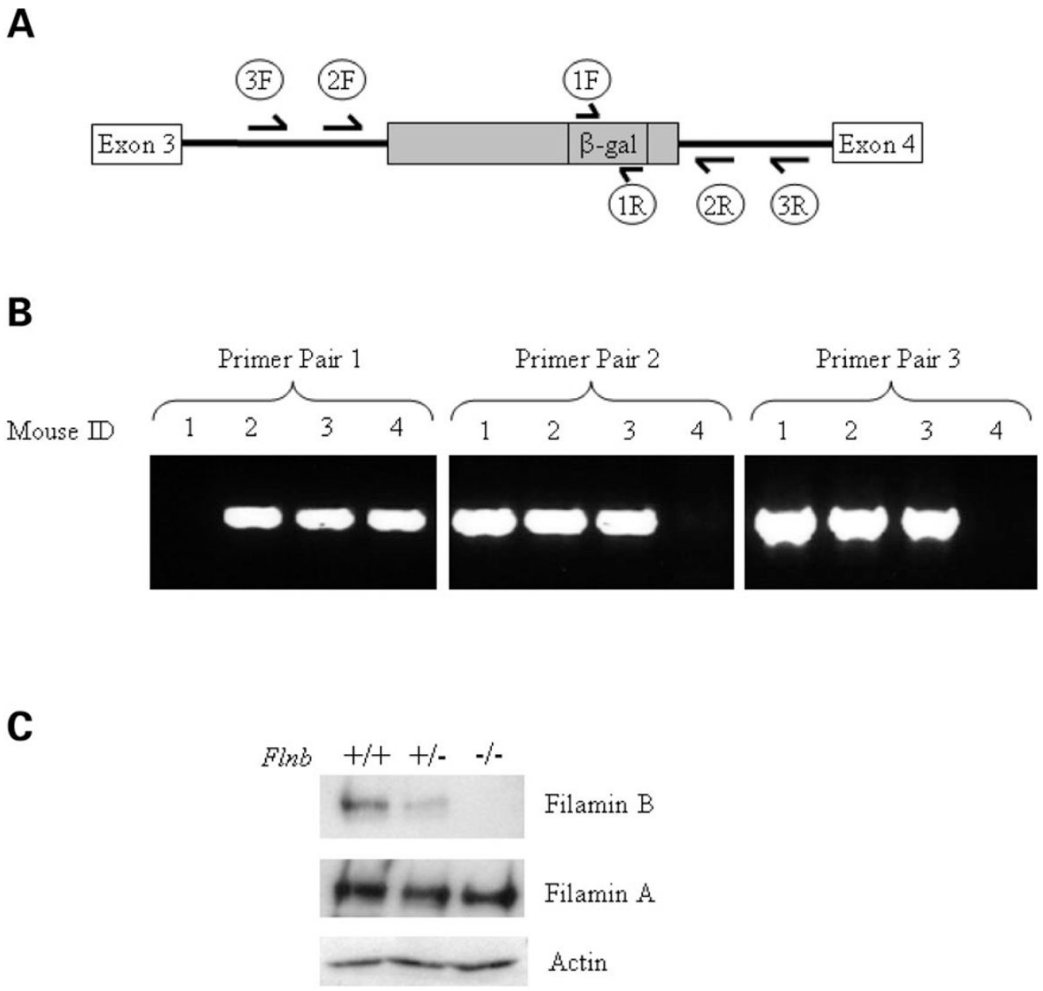

Figure 3.

(**A**) Schematic diagram showing the location of the oligonucleotide pairs used to genotype the *Flnb*$^{-/-}$ mice. The gene-trap vector (gray box) insertion site is in intron 3 of *Flnb* (black line) and contains the reporter gene β-galactosidase (β-gal). Oligonucleotide pair 1 (1F and 1R) amplify sequences in the β-gal gene, oligonucleotide pairs (2F and 2R) and (3F and 3R) amplify sequences within intron 3 of *Flnb* 5′ and 3′ to the gene-trap vector. (**B**) An example of genotyping results obtained from the PCR amplification of genomic DNA of four mice using the oligonucleotides shown in (A). Results show that the genotype of mouse 1 is *Flnb*$^{+/+}$, mice 2 and 3 is *Flnb*$^{+/-}$ and mouse 4 is *Flnb*$^{-/-}$. (**C**) Western blot analysis of filamin B (top panel) and filamin A (middle panel) from a *Flnb*$^{+/+}$ mouse (lane 1), a *Flnb*$^{+/-}$ mouse (lane 2) and a *Flnb*$^{-/-}$ mouse (lane 3). The bottom panel shows actin expression to demonstrate protein loading.

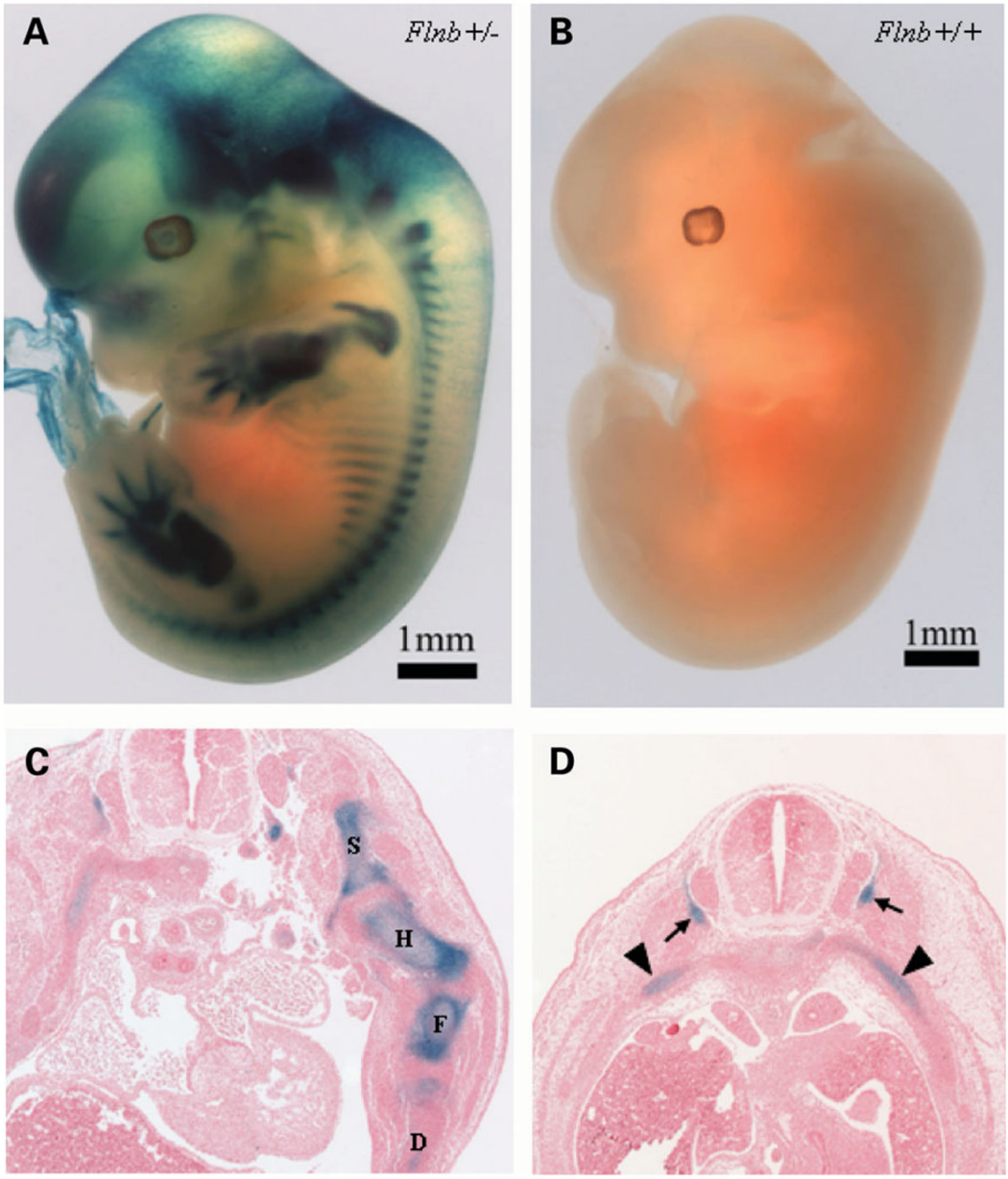

Figure 4.
Filamin B expression (blue stain) in E12.5 embryos on a whole mount *Flnb*$^{+/-}$ mouse (**A**), a whole mount *Flnb*$^{+/+}$ mouse (**B**) and sections from a *Flnb*$^{+/-}$ mouse (C, D). (**C**) shows a transverse section through the upper thorax and forelimb. Filamin B expression is seen in the developing scapula (S), humerus (H), ulna and radius (U/R) and the digits (D). (**D**) shows a transverse section through the trunk showing filamin B expression in the neural arch of the developing vertebrae (arrows) and the ribs (arrow heads).

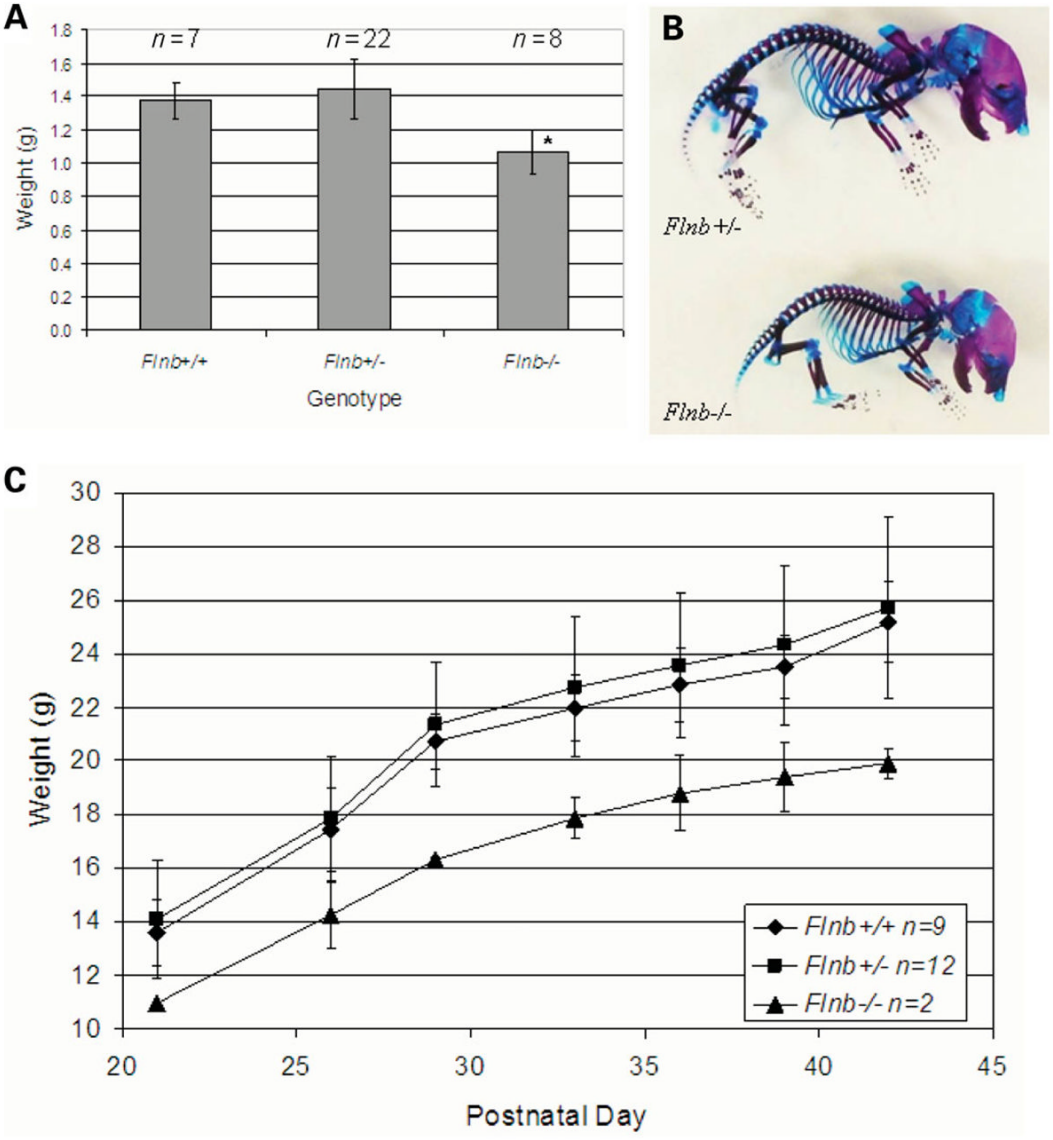

Figure 5.

(**A**) Graphical representation of the weights of newborn mice compared with their genotypes. *$P < 0.05$. (**B**) Skeletal preparation of newborn mice. Bone is stained with alizarin red S and cartilage is stained with alcian blue. (**C**) Graphical representation of the weights of male mice from postnatal day 21 over a 3-week period compared with their genotypes.

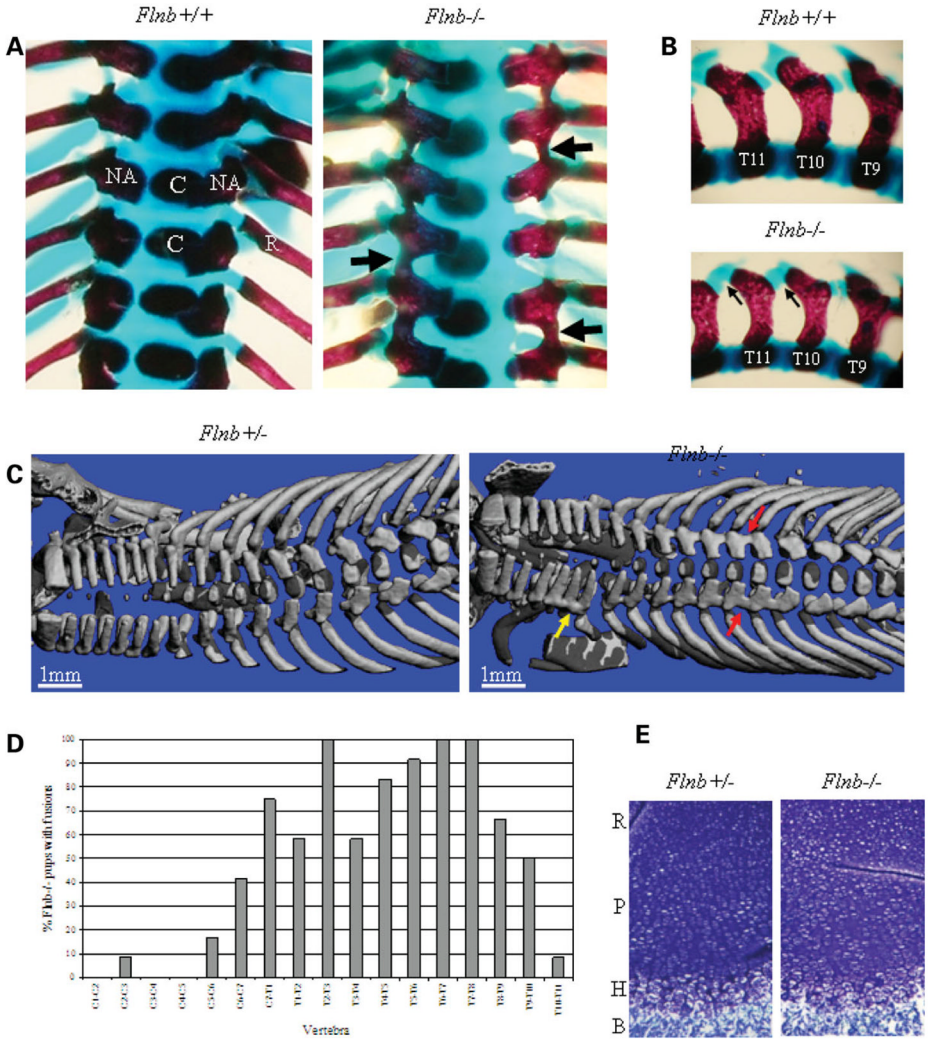

Figure 6.

(**A**) Dorsal view of the thoracic spine in skeletal preparations of newborn mice with different genotypes. Arrows show regions of mineralization between the neural arches (NA) of the vertebrae in the *Flnb*$^{-/-}$ mice. The mineralization center of the centra (C) and the ribs (R) can also be seen. (**B**) Lateral view of the thoracic vertebrae T9–T11 (right–left) in skeletal preparation of newborn mice. The arrows show fused cartilage of the superior and inferior articular processes on the neural arches in the *Flnb*$^{-/-}$ mice. (**C**) Dorsal view of a micro-CT three-dimensional reconstruction of newborn mice. Fusions can be seen between the neural arches of the cervical vertebrae (yellow arrow) and thoracic vertebrae (red arrows) in the *Flnb*$^{-/-}$ mice. (**D**) Graph to show which vertebrae were fused in the *Flnb*$^{-/-}$ mice (n = 12 with both sides of each neural arch being counted separately). (**E**)Toluidene blue stained sections of distal femur growth plate in newborn littermates showing the reserve zone (R), proliferative zone (P), hypertrophic zone (H) and bone (B).

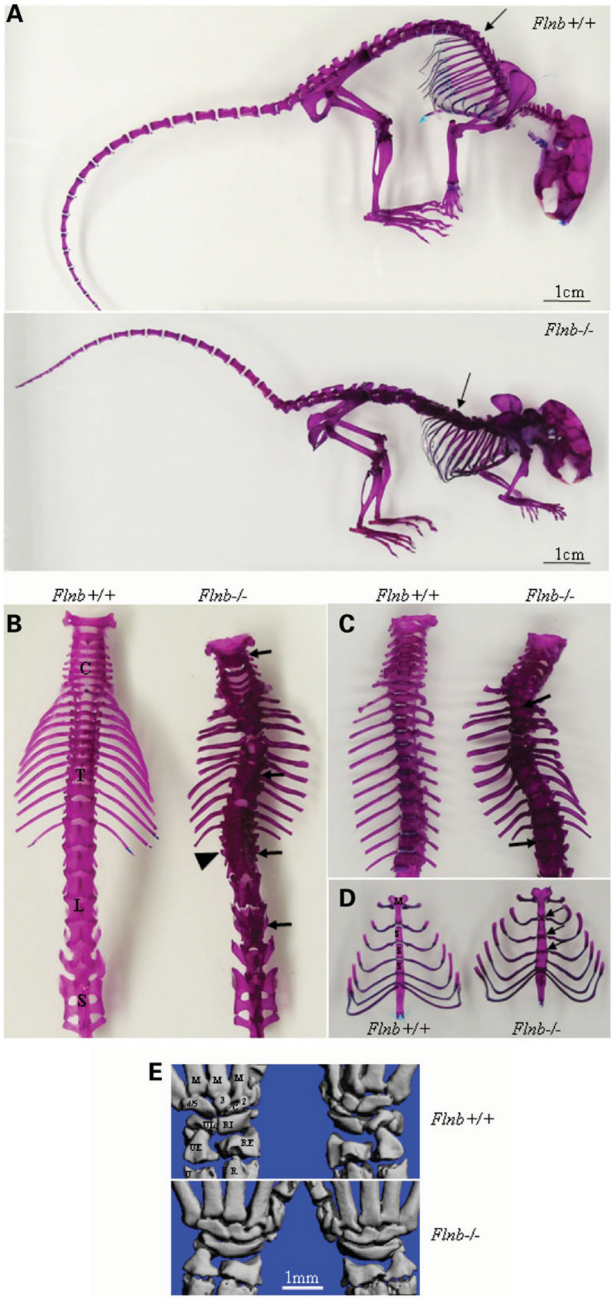

Figure 7.

(**A**) Whole skeletal preparation of female mice at postnatal day 60. Fusions in the vertebrae of the *Flnb*$^{-/-}$ mice cause a flattening of the spine compared with *Flnb*$^{+/+}$ mice (arrow). (**B**) Dorsal views of the disarticulated skeletons shown in (A). Fusions are present in the cervical, thoracic and lumbar regions of the *Flnb*$^{-/-}$ mouse (arrows). Transverse processes can still be seen in some of the fused vertebrae (arrowhead). C, cervical; T, thoracic; L, lumbar; S, sacrum. (**C**) Ventral views of the disarticulated skeletons shown in (A). Fusion are present between the centra in the *Flnb*$^{-/-}$ mouse (arrows). (**D**) Sterna of the mice is shown in (A). Fusions are present between the sternebrae (S) and the manubrium (M) in the *Flnb*$^{-/-}$ mice (arrows). (**E**) Comparison of micro-CT three-dimensional reconstruction of the left and right manus of

Flnb$^{+/+}$ and *Flnb*$^{-/-}$ mice at postnatal day 60. U, ulna; UE, ulna epiphysis; UL, ulnare; R, radius; RE, radial epiphysis; RI, fused radiale and intermedium; 2, second distal carpal; C, centrale; 3, third distal carpal; 4/5, fourth and fifth distal carpals; M, metacarpal.

Table 1

Nonsense mutations identified in the coding region of *FLNB*[a]

Patient	DNA mutation	Exon	Amino acid substitution	Filamin B domain
1[b]	c.1945C > T	13	p.Arg649X	5
2[b,c]	c.2452C > T and c. 4819C > T	16 and 28	p.Arg818X and p.Arg1607X	6 and 14
3[b]	c.6408delC	39	p.Ser2137LeufsX4	20
4[b,c]	c.7029T > G	43	p.Tyr2343X	22
5	c.5548G > T	33	p.Gly1850X	17
6[c]	c.1945C > T and c. 4671G > A	13 and 27	p.Arg649X and p.Ser1505ArgfsX33	5 and 14
7	c.6010C > T	36	p.Arg2004X	19

[a] The cDNA sequence of *FLNB* was based on GenBank number NM_001457 and nucleotide numbering is from the start of translation (i.e. +1 corresponds to A of the ATG translation initiation codon in the reference sequence and the initiation codon is codon 1).

[b] Mutations previously reported (4).

[c] Patient samples used in filamin B expression studies.